Continuity of the poleward undercurrent along the eastern boundary of the mid-latitude north Pacific

S.D. Pierce[a,*], R.L. Smith[a], P.M. Kosro[a], J.A. Barth[a], C.D. Wilson[b]

[a]*College of Oceanic and Atmospheric Sciences, Oregon State University, 104 Ocean Administration Bldg., Corvallis, OR 97331-5503, USA*
[b]*NOAA-NMFS, Seattle, WA 98115-0070, USA*

Abstract

Several recent data sets improve our view of the poleward undercurrent of the California Current System. As part of a triennial National Marine Fisheries Service (NMFS) survey of Pacific whiting, a series of 105 shipboard acoustic Doppler current profiler (ADCP) velocity sections across the shelf break from 33 to 51°N at about 18 km meridional spacing were collected from July to August 1995. Significant ($> 0.05 \, \mathrm{m \, s^{-1}}$) subsurface poleward flow occurred in 91% of the sections. A mean cross-shelf section using the entire data set has statistical significance, revealing an undercurrent core $> 0.1 \, \mathrm{m \, s^{-1}}$ from 200–275 m depth 20–25 km off the shelf break. The mean poleward volume transport in a 125–325 m layer is $0.8 \pm 0.2 \times 10^6 \, \mathrm{m^3 \, s^{-1}}$. We focus particular attention on the Cape Blanco to Cape Mendocino region, and the NMFS results are compared with shipboard ADCP three weeks later from a study of coastal upwelling processes near Cape Blanco. ADCP streamfunction maps are derived and strongly suggest that one portion of flow is continuous over the 440 km meridional extent of the analysis region. Other portions of the flow show evidence of offshore turning, separation, and the formation of anti-cyclonic eddies. We also note that isopycnic potential vorticity from alongslope CTD stations during the NMFS survey appears to be a tracer for the poleward flow. © 2000 Elsevier Science Ltd. All rights reserved.

---

* Corresponding author.
E-mail address: spierce@oce.orst.edu (S.D. Pierce).

1. Introduction

Subsurface poleward flow occurs along all five major oceanic eastern boundaries. At mid-latitudes, this poleward flow opposes the equatorward subtropical eastern boundary current flow at the surface. During the coastal upwelling season, the poleward flow also opposes intense equatorward surface-intensified upwelling jets. These undercurrents are usually found over the continental slope and have typical alongshore speeds of 0.1–0.3 m s^{-1} and a depth range 100–300 m (Neshyba et al., 1989; Warren, 1990). Since they have volume transports of O(1) $\times 10^6$ m^3 s^{-1}, they may be significant oceanic features in a global circulation context, besides being important aspects of eastern boundary regions.

Although the poleward undercurrent in the California Current System has been the best observed and most studied of any, several basic dynamic and kinematic issues remain unresolved (e.g. Warren, 1990). Some of the outstanding kinematic questions concern the undercurrent's continuity in both space and time. Most historical observations have consisted of individual cross-shore hydrographic sections and relatively short current meter records. Some of the most interesting recent observations of the poleward undercurrent have been Lagrangian measurements using subsurface RAFOS drifters (Collins et al., 1996a). These measurements unambiguously demonstrate the continuity of the poleward flow at about 140 m depth over a 500 km path from 37.8 to 41.8°N.

The 1995 triennial acoustic-trawl survey by the National Marine Fisheries Service (NMFS), to assess the abundance and distribution of Pacific whiting, included shipboard acoustic Doppler current profiler (ADCP) velocities, which we examine here. The fisheries results are reported by Wilson and Guttormsen (1997). The effects of currents on Pacific whiting are also under investigation and will be reported elsewhere. The survey sampled the entire mid-latitude eastern Pacific slope in July–August 1995, with cross-slope transects running nominally from 50 to 1500 m isobaths at 18 km meridional spacing (Fig. 1). Although the cruise plan was largely determined from fisheries considerations, the data set is also well-suited to studying the poleward undercurrent.

The meridional extent of the NMFS ADCP data allows us to address issues of spatial continuity and latitudinal variation. Also in 1995, three weeks after the NMFS survey passed Oregon, an intensive SeaSoar/ADCP survey studied upwelling processes at Cape Blanco (Barth et al., 2000; Barth and Smith, 1998). We present some results from this survey, which observed strong interaction between the poleward undercurrent and a separating coastal upwelling jet above.

In the presence of tidal currents and inertial oscillations, and with little concurrent cross-shore hydrographic data, we seek to detect the subtidal and relatively stable and geostrophic poleward undercurrent. We accomplish this primarily using two methods: averaging together many cross-shore sections to reduce the "noise", and deriving streamfunction to help reveal the non-divergent subtidal velocity field.
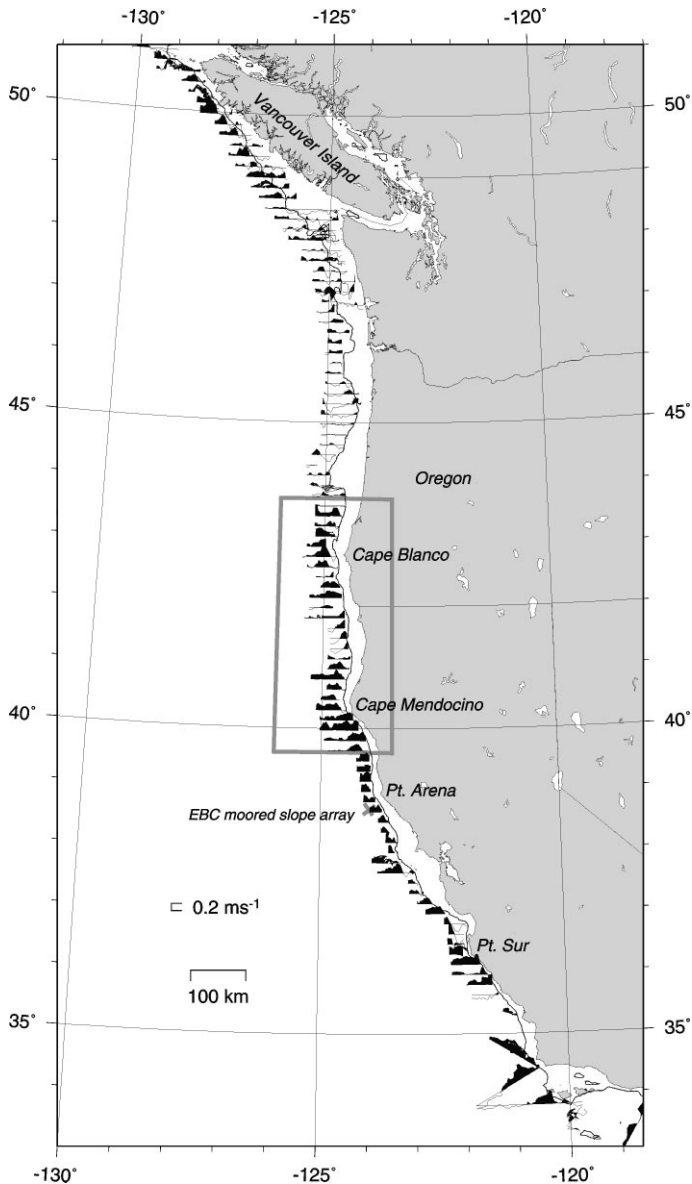
Fig. 1. ADCP transects across the shelf break during the NMFS Pacific whiting survey, July–August 1995. Depth-averaged subsurface alongshore flow between 125 and 325 m is plotted normal to the ship track, with poleward flow shaded. The 200 m isobath is shown.

2. Data and methods

Surveys to assess the abundance and distribution of Pacific whiting have been conducted every three years since 1977 by the NMFS. The survey in 1995 was by the

R/V *Miller Freeman* and included acoustic echo measurements at two frequencies (38 and 120 kHz) using a Simrad EK500 system, as well as trawl work. The complete 1 July–1 September 1995 survey included a fast run down to the southern end from Seattle at the beginning and additional transects from 52 to 55°N off the Queen Charlotte Islands at the end. Results here use data from 7 July to 28 August between 33 and 51°N (Fig. 1). Nominal meridional spacing of these 105 mostly east–west lines was 18 km, and the mean length of a transect was 52 km. Transects generally ran mid-shelf to mid-slope, between the 50 and 1500 m isobaths, sometimes extending to deeper water depending on real-time biological scattering results (Wilson and Guttormsen, 1997). CTD casts were made at selected trawl sites and at two or three locations along every second or third transect, down to depths of about 500 m. For the first time, this Pacific whiting survey also included acoustic Doppler current profiler (ADCP) velocity measurements.

The CTD data are used to compute "spiciness" as defined by Flament (1986). Spiciness is approximately perpendicular to σ_θ in a T–S diagram and works well in the California Current System because average T–S curves lie roughly orthogonal to isopycnals (Tibby, 1941). High spiciness corresponds to high temperature or high salinity, while low spiciness corresponds to low temperature or low salinity. Temperature and salinity, hence spiciness, on subsurface isopycnals can be assumed to be conservative. Density anomaly sigma–theta (σ_θ) was calculated using the 1980 EOS algorithms.

An RD Instruments 153.6 kHz narrow-band, hull-mounted ADCP measured currents throughout the survey. We used a vertical bin width of 8 m, pulse length of 8 m, and an ensemble averaging time of 2.5 min. Pings per ensemble varied from 66 to 101, and the depth range of good data (good pings > 30%) was typically 22–326 m. Details of ADCP data processing generally follow the methods used for the R/V *Wecoma* Cape Blanco study (Barth et al., 2000), which are contained in the data report Pierce et al. (1997). Data were required to pass tests of sufficient return signal, acceptable second derivatives of $u, v,$ and w with respect to depth, and reasonable error velocities, as recommended by Firing et al. (1995) and Zedel and Church (1987). The ADCP was slaved to the EK500 biological instrument to avoid interference. Precruise tests revealed no interference between the two instruments when the ADCP obtained ship velocity from navigation alone. The ADCP bottom-tracking feature, however, which puts more energy into the water, was found to cause an artificial signal on the EK500. For this reason, bottom tracking was never enabled throughout the survey. GPS P-code (military-type) navigation was used for position and gyrocompass for heading, to determine absolute velocities. The ADCP/navigation/gyrocompass system was calibrated by covariability between currents and ship velocity (Kosro, 1985; Pollard and Read, 1989). A scale factor of 2% and a calibration error, which varied linearly in time from 0.1 to 0.5°, were detected and removed. Remaining calibration uncertainty implies an unknown bias of $0.02 \, \mathrm{m \, s^{-1}}$ in absolute velocities. Raw reference layer velocities were low-pass filtered with a 20 min Blackman window (Firing et al., 1995). Short-term inherent random errors for an ensemble are at most $0.02 \, \mathrm{m \, s^{-1}}$, and the estimated rms error in absolute reference layer velocity is $0.04 \, \mathrm{m \, s^{-1}}$.

Sections of ADCP were contoured using a four-pass Barnes objective analysis (OA) scheme (Barnes, 1994; Daley, 1991). The Barnes scheme, widely used in atmospheric

science, applies a Gaussian-weighted average successively, converging towards the observed points. The method is related to statistical optimal interpolation, but is simpler and more flexible and does not require prior specification of a covariance model for the observed field. Statistical optimal interpolation is only "optimal" for a given covariance model; the lack of sufficient historical data frequently makes determination of the appropriate model difficult. Four Barnes iterations were sufficient, since at this point the gridded values were changing $< 0.01 \, \mathrm{m \, s^{-1}}$ rms. We hold the Barnes radii constant at 7.5 km in the horizontal and 25 m in the vertical; scales larger than these are not smoothed.

We define an approximate alongshore direction to be 330°T south of 40.2°N and north of 48°N, and 0°T from 40.2 to 48°N. For maps of ADCP vectors, component values and locations are 5 km spatial averages, and in cases where the cruise track overlays itself, measurements from different times are averaged together.

We derive streamfunction from the ADCP velocities. This helps reveal the undercurrent by reducing the aliasing effects of tidal and inertial signals. First, the two components of velocity are gridded using a four-pass Barnes OA (Barnes, 1994). Both the alongshore and the offshore Barnes radii are kept constant at 18 km, which is the alongshore sampling interval. This choice minimizes unnecessary smoothing of the resulting fields, which is appropriate here since we are deriving streamfunction as a descriptive tool, rather than selecting certain length scales based on dynamical ideas. We determine streamfunction over this gridded velocity field using the version III method of Hawkins and Rosenthal (1965), introduced to the oceanographic community by Carter and Robinson (1987). A Poisson equation for the velocity potential, forced by the observed field of divergence (calculated for each grid box), is solved with a boundary condition of zero on all sides. The resulting velocity potential is then used to add a correction to the boundary conditions for the Poisson equation for the streamfunction, forced by the relative vorticity field. This approach has the effect of maximizing the amount of kinetic energy in the resulting streamfunction field. We use the Poisson solver developed by Cummins and Vallis (1994), which handles the irregular boundary condition of no normal flow into the coast. Attempting to use the observed velocity field directly as a boundary condition for the streamfunction calculation, the simplest approach (e.g. Pollard and Regier, 1992; Allen and Smeed, 1996), implicitly assumes that the observed field along the boundary is non-divergent, which may not be true given measurement noise. Non-divergent vectors are derived from the gridded streamfunction and then interpolated back to their original locations using improved Akima bivariate interpolation (Akima, 1996). The Barnes OA and the streamfunction derivation together amount to a method of systematically applying conservation of mass throughout a region.

3. Southern California to Vancouver Island

The full set of 105 alongshore velocity sections from the NMFS survey are available for viewing in an on-line data report (Pierce, 1997). Here we present a representative sample of 16 sections (Fig. 2a and b). As expected during the summer upwelling season, surface equatorward flow is frequently present. Significant surface-intensified
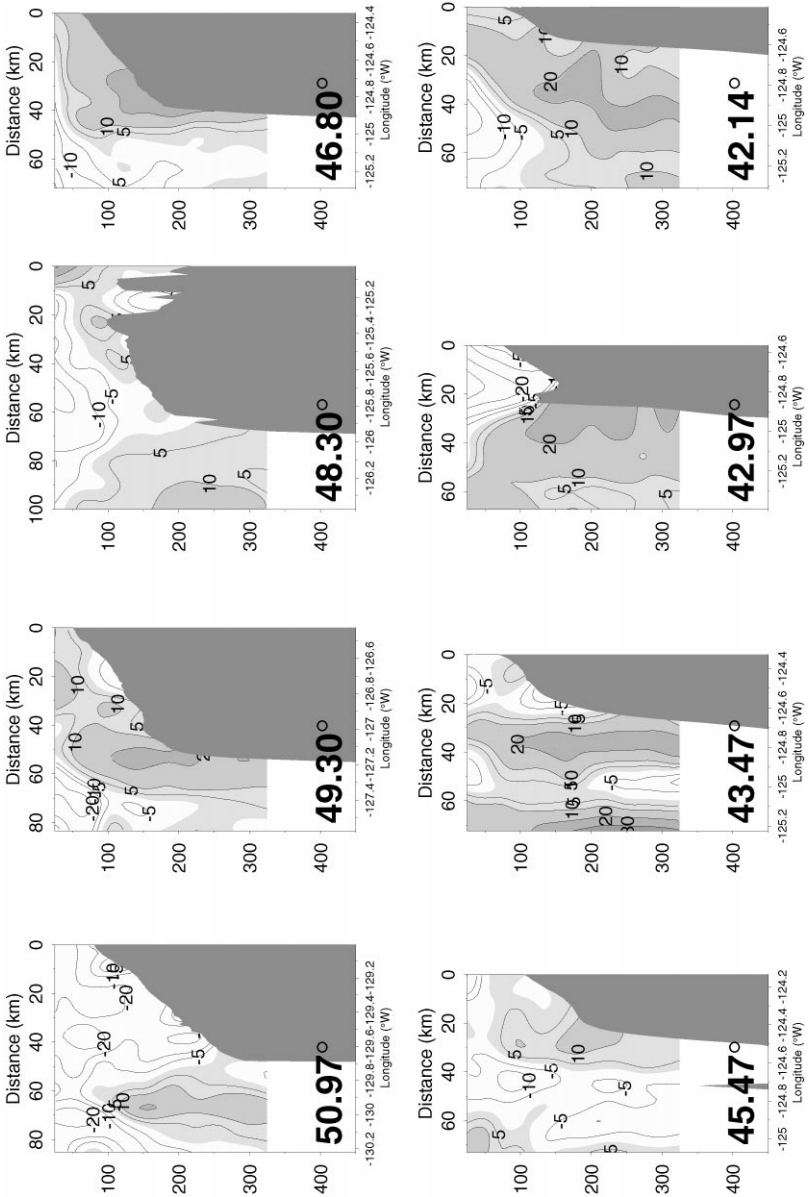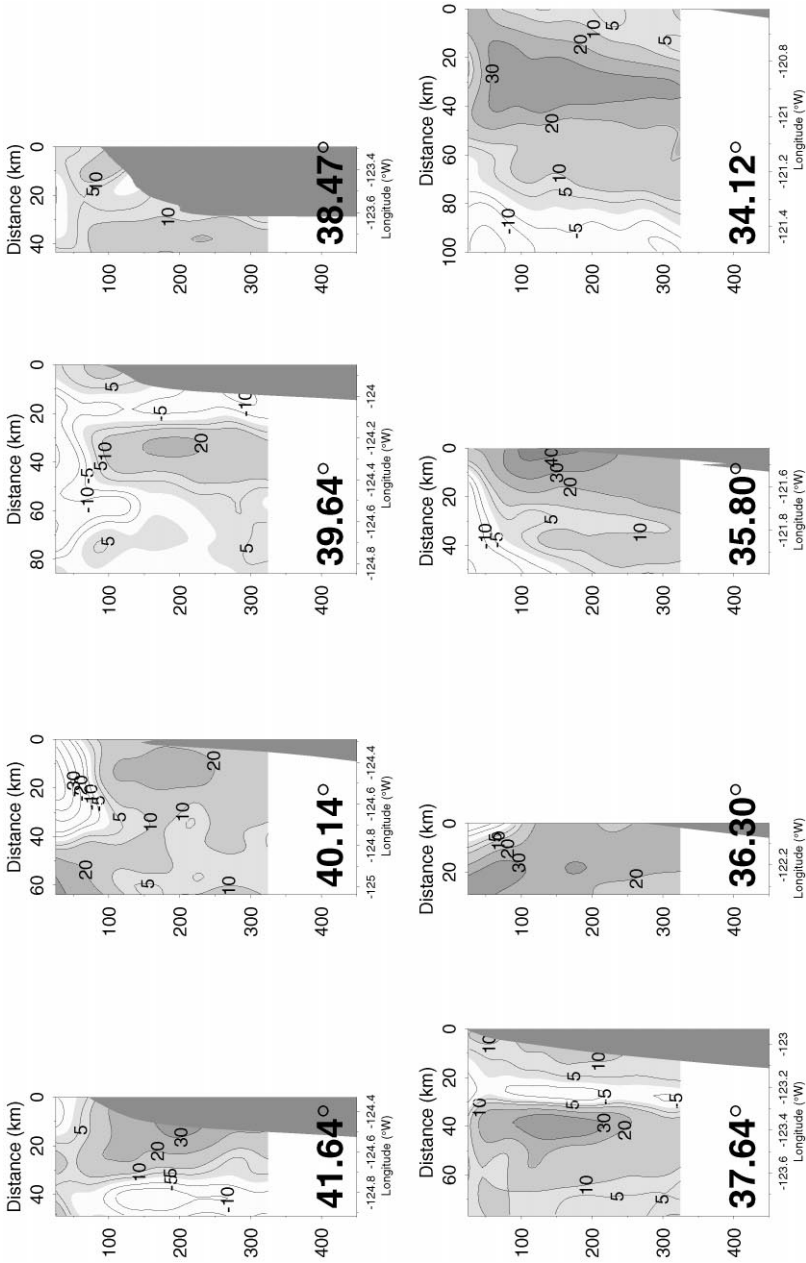
Fig. 2. Selected ADCP vertical sections of alongshore flow (cm s^{-1}). Poleward flow is shaded.

equatorward jets associated with upwelling can be seen at 48.3°N, 42.97°N, 42.14°N, and 40.14°. Consistent with historical observations and satellite imagery (Smith, 1995), the upwelling jets to the north of 42.8°N (Cape Blanco, Oregon) appear to be confined inshore of the continental shelf break. In sections to the south of 42.8°N, the upwelling jets can be found seaward of the shelf break. The separation, that occurs as an upwelling jet passes through this region, can be seen by comparing the 42.97°N and 42.14°N sections. Observation of the details of this separation process was the motivation for the Cape Blanco study (Fig. 7; Barth et al., 2000). Outside of this region, the absence of many cross-shore hydrographic observations to complement the NMFS ADCP makes further interpretation of the surface flows difficult. In this paper we focus on the subsurface poleward flow.

The ubiquity of poleward flow throughout the 5400 km of cross-shore trackline is striking. Individual sections show complex poleward current patterns (Fig. 2). Barotropic tidal currents, baroclinic tidal currents, and inertial oscillations are probably all present in any particular section, a 0.05–$0.10 \, \text{m s}^{-1}$ contribution (Torgrimson and Hickey, 1979) which confuses the view of the subtidal and geostrophic signal.

As one method of summarizing this large data set, we consider a subsurface depth-averaged layer from 125 to 325 m (Fig. 1). We chose this layer definition as a reasonable one to focus our attention on the subsurface poleward undercurrent. Depth-averaged poleward flow within this subsurface layer appears as black shading in Fig. 1. In 96 out of 105 sections, maximum velocity is at least $0.05 \, \text{m s}^{-1}$ over a 5 km width. The mean of the maximum core layer velocities seen at each section is $0.18 \pm 0.01 \, \text{m s}^{-1}$.

3.1. Mean structure

One approach to the problem of separating out the undercurrent signal from other processes is to form averages. The effects of tides, inertial oscillations, and other phenomena will decrease as sections are averaged. The sections were not in general sampled on a schedule close to a tidal periodicity. We have sufficient realizations and the undercurrent core is stable enough to render meaningful such a meridional mean section (Fig. 3). The entire NMFS ADCP data set (including connecting legs between transects) is regridded (using 5 km grid spacing) onto an off-shelf-break coordinate system, then contoured (Fig. 3). Standard errors (assuming $N = 105$ independent points) are figured for each grid point, and these are less than $0.02 \, \text{m s}^{-1}$ (Fig. 3). The mean cross-shelf section reveals a poleward undercurrent core $> 0.10 \, \text{m s}^{-1}$ with thickness 200–275 m, 20–25 km off the shelf break (Fig. 3). The mean poleward volume transport below 125 m is $0.8 \pm 0.2 \times 10^6 \, \text{m}^3 \, \text{s}^{-1}$.

In addition to this evidence of the alongshore continuity of the undercurrent, recent results from an array of moorings provide evidence of its continuity in time: the Eastern Boundary Current moored array at 38.5°N measured currents for 22 months at five cross-shore locations extending from the inner slope (410 m) to the abyssal plane (3650 m), at 14 km spacing (Kosro et al., 1994). Mean poleward flow was observed at depths > 100 m, with maximum poleward flow of $0.11 \, \text{m s}^{-1}$ at the innermost mooring at about 175 m.
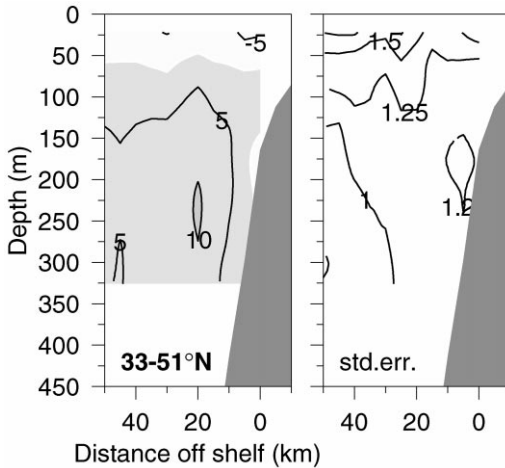
Fig. 3. Spatial mean section of alongshore flow using all NMFS ADCP data, after transformation into an off-shelf coordinate system, using distance from the 150 m isobath. Right panel shows corresponding standard error of the mean.

From a single current meter at 350 m depth located over the 800 m isobath off Pt. Sur, a relatively long (six year) time series is available (Collins et al., 1996b). Again, the $0.08 \, \text{m s}^{-1}$ poleward flow from the moored instrument at 350 m agrees well with our $0.09 \, \text{m s}^{-1}$ mean at 325 m.

3.2. Meridional trends

Both the subsurface poleward maximum layer velocities and the layer transports for individual sections show significant scatter (Fig. 4). This is not surprising, given the presence of unresolved tidal, inertial, and other phenomena. We initially determined a statistically significant large-scale trend with latitude in both characteristics, by classical least-squares fits (dashed lines of Fig. 4), as in Pierce et al. (1996). Both the core velocities and the transports decrease poleward.

Although these trends are significant at the 95% level, this is not necessarily the appropriate model. We noticed first by eye, particularly in the transport, a region 43–47°N with reduced values. We then experimented with the variable block aver-aging (VBA) filter of Howell (1995), a type of adaptive filter specifically designed to identify sharp boundaries in geophysical data. The VBA algorithm uses information obtained by applying the Haar transform (a primitive wavelet) on a fixed scale and at all possible positions within the data record. The solution is the one with the greatest skill, among all possible solutions that could be constructed using any number of blocks of size $n = 18$ or greater.

The VBA confirms a transition located just north of Cape' Blanco, in both core velocity and transport. The location of this transition is consistent with the location of the equatorward surface jet separation in the Cape Blanco region (Barth et al., 2000).
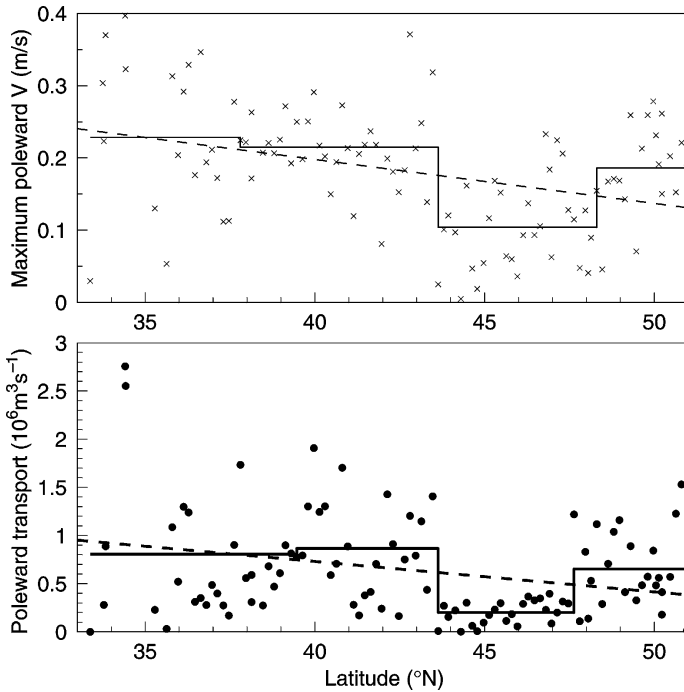
Fig. 4. Maximum poleward V ($\times$) and the total subsurface layer transport ($\bullet$), for each NMFS ADCP section. Light and bold solid lines show variable block averages for the maximum V and transport respectively. Light and bold dashed lines are least-squares fits.

Anticipating the results of the next section as seen in Fig. 7, and discussed in detail in Barth et al. (2000), a separating coastal jet can strengthen and deepen to the point where it interacts significantly with the poleward undercurrent. To the north of 47°N, core velocity and transport are similar to what they were to the south of Cape Blanco. Excluding 43–47°N, we see only a small decrease in the core velocity and transport of about 1% per degree of latitude.

The characteristic width of the undercurrent (defined as the width at half-maximum velocity) and its change with latitude are revealed by forming three mean sections (Fig. 5). Using two 5° latitude bands to the south of Cape Blanco and one 4° band to the north, a narrowing of the undercurrent to poleward is evident, although barely statistically significant given uncertainties in width estimation (probably ± 5 km). Consistent with the undercurrent hugging the slope, the core moves closer to the slope as it narrows. The first-baroclinic Rossby radii of deformation for these latitude bands, as calculated by Chelton et al. (1998) from climatological 1° gridded hydrographic data, are 24.3, 21.8, and 15.5 km (Fig. 5, horizontal lines). The widths of the poleward flow are consistent with the Rossby radii, which has also been noted in the case of the Peru undercurrent (Huyer, 1980). The change in width is not connected with a change in bottom slope, which does not change systematically with latitude.
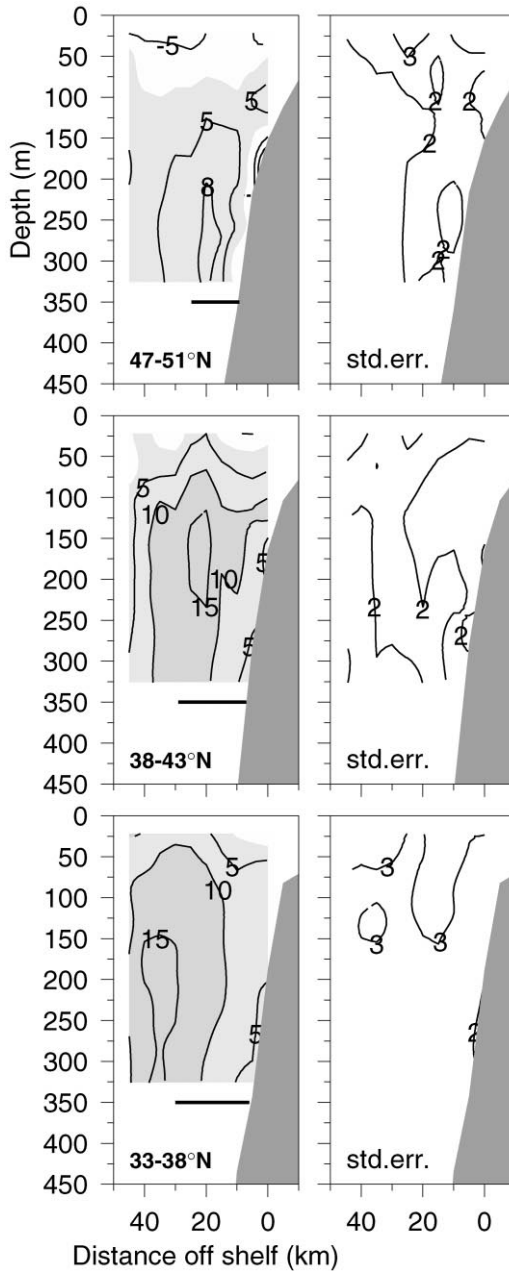
Fig. 5. Spatial mean sections for three different latitude bands. The horizontal line just below each section indicates the first baroclinic Rossby radius of deformation length, calculated from climatology within the same latitude band (from Chelton et al., 1998). Right panels show corresponding standard errors for each mean.

The first-baroclinic Rossby radius is a natural length scale in the ocean, and it is often associated with widths of boundary phenomena such as coastal upwelling, Kelvin waves, etc. It is not surprising that the poleward undercurrent flow appears to be related to this scale as well.

4. Cape Mendocino to Cape Blanco

We focus now on the Cape Mendocino to Cape Blanco region (Fig. 6a). We choose this area to apply our method of deriving streamfunction from the ADCP data. This area is of particular interest since Cape Blanco appears to be the northernmost point where a surface equatorward jet separates from the coast and remains seaward of the shelf to become a meandering jet characteristic of the California Current System (Barth et al., 2000). It is also a region where the NMFS transects fortunately extended further offshore than usual (Fig. 1), beyond the 2000 m isobath, allowing us to resolve some of the flow field along the offshore edge of the undercurrent.

The original 5 km NMFS ADCP vectors for the subsurface layer (125–325 m) clearly show poleward flow, but the presence of other oceanic phenomena is also obvious (Fig. 6a). The Barnes OA smoothing and the enforcement of non-divergence reduce the aliasing effects of tidal and inertial signals, retaining any subtidal mesoscale flow such as the poleward undercurrent (Fig. 6b). This amounts to a method of systematically applying conservation of mass throughout the region. The streamfunction plotted underneath has contour intervals corresponding to $0.1 \times 10^6 \, \mathrm{m^3 \, s^{-1}}$ in transport.

At least $0.3 \times 10^6 \, \mathrm{m^3 \, s^{-1}}$ of the transport unambiguously transit the 440 km alongshore length of our region, on the inshore side. Offshore of this, other portions of the flow are more complex, with evidence of meandering and eddy formation. At 41.2°N, for example, part of the undercurrent is turning offshore, and this appears to be part of an anticyclonic eddy that is just about to break away. At 42°N the current meanders westward; this might be an early stage of an eddy formation process.

This view of the undercurrent, as a combination of some continuous flow inshore and another portion offshore prone to instabilities and anticylconic eddy formation, is consistent with recent Lagrangian measurements using subsurface RAFOS drifters (Collins et al., 1996a; Garfield et al., 1999). Both their floats #5 and #19 experience an acceleration and a veering offshore in the vicinity of Cape Mendocino, followed by a deceleration and gradual return onshore to the north, similar to our streamlines. Float #19 then drifts westward to the north of Cape Mendocino in similar fashion to the flow we see at 41.2°N. Float #5 traces a path through most of the region quite similar to our continuous streamlines, remaining in the undercurrent hugging the coast until just south of 42°N. At this point it heads offshore and gets caught in an anticyclonic eddy of about 35 km diameter, centered at about 125.2°W, 42.3°N. The meander we observe at 42°N might be the start of a process leading to such an eddy. Huyer et al. (1998) in the Eastern Boundary Current experiment also describe offshore subsurface anticyclonic lenses of relatively spicy water, which were presumed to form from the undercurrent in this manner and then drift to the west.
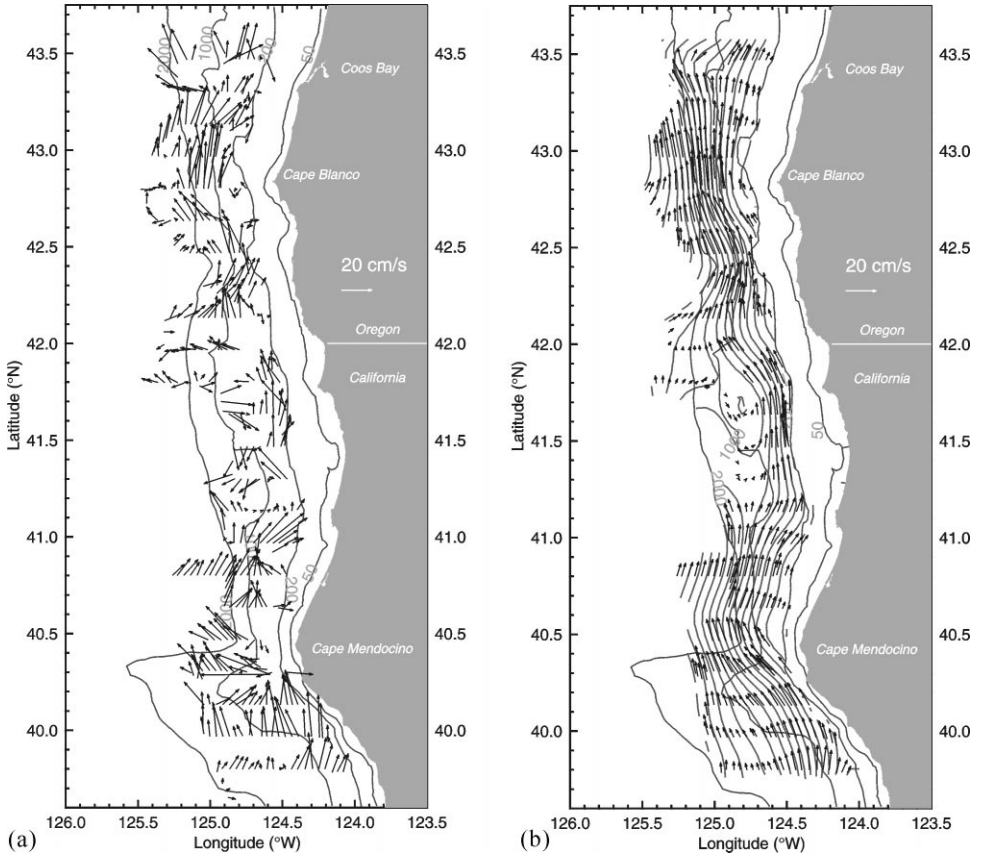
Fig. 6. (a) Observed ADCP velocity vectors (depth-averaged 125–325 m) from the NMFS survey, obtained during 21–29 July 1995. (b) Non-divergent ADCP velocity vectors for the same subsurface layer. The gray shade lines underneath are the corresponding transport streamfunction contours, with a $0.1 \times 10^6 \, \text{m}^3 \, \text{s}^{-1}$ contour interval.

About three weeks after the large-scale survey (17–27 August 1995), an intensive SeaSoar/ADCP survey of the Cape Blanco region took place (Fig. 7a; Barth et al., 2000). Again there is a significant portion $(0.2 \times 10^6 \, \text{m}^3 \, \text{s}^{-1})$ of the flow that is continuous poleward through the region (Fig. 7b). This time, however, another $0.5 \times 10^6 \, \text{m}^3 \, \text{s}^{-1}$ of the undercurrent entering from the south turns offshore and then equatorward. This is due to contact with a strong equatorward upwelling jet that separates from the coast off Cape Blanco, strengthens, and deepens to the point where it interacts with the top of the poleward undercurrent. Barth et al. (2000) examine this interaction in detail. Relatively spicy undercurrent water can be seen interacting with and becoming part of the equatorward surface jet (their Fig. 9). Three weeks previously (the NMFS survey passed through the region 25–30 July 1995), a smaller separated upwelling jet existed (Fig. 2, 42.14°N), but this did not interact significantly
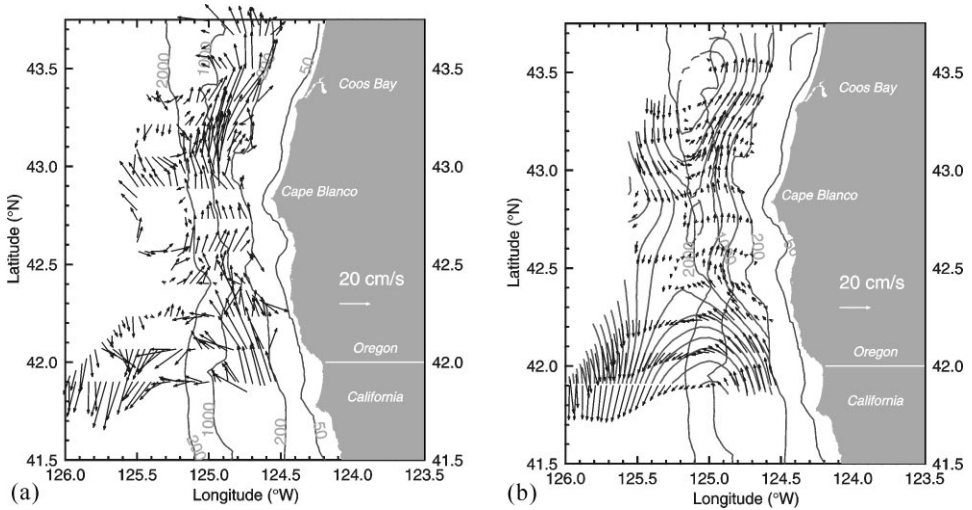
Fig. 7. (a) Observed ADCP velocity vectors (depth-averaged 125–325 m) from the Coastal Jet Separation during 17–27 August 1995 cruise. (b) Non-divergent ADCP velocity vectors for the same subsurface layer. The gray shade lines underneath are the corresponding transport streamfunction contours, with a $0.1 \times 10^6 \, \text{m}^3 \, \text{s}^{-1}$ contour interval.

with the undercurrent. The interaction with a strong separating surface jet above is another mechanism for a portion of the undercurrent to turn offshore.

5. Alongslope hydrography

As part of the NMFS survey, CTD casts were made at two or three locations along every second or third transect, down to depths of about 500 m. We selected the 31 stations out of the total of 65 that were on the slope (bottom depths 245–1830 m) to characterize the meridional water mass properties of the undercurrent. The core of spicy water at 100–250 m at the southern end of the survey spreads to poleward and is still detectable as a spiciness maximum in the vertical at the northern end of the survey, at 150–225 m depth (Fig. 8a). Several examples of this type of indirect evidence for poleward undercurrent flow can be found in Neshyba et al. (1989).

The Cape Blanco study made a cross-slope CTD section at 43.2°N, the FM line (Fig. 9a). Here the down-warped $\sigma_\theta = 26.6$ isopycnal close to the slope indicates the presence of poleward geostrophic flow, and the spiciness maximum confirms the southern source of this undercurrent flow.

Also shown in Fig. 8a (small triangles) is the depth of the center of mass of poleward flow from ADCP. This is calculated as $z_{\text{cm}} = \sum vz / \sum v$ over the subsurface layer, where v is a raw poleward ADCP velocity and z is the depth of that measurement, providing a good indication of the core undercurrent depth. We note that z_{cm} ranges from 150 to
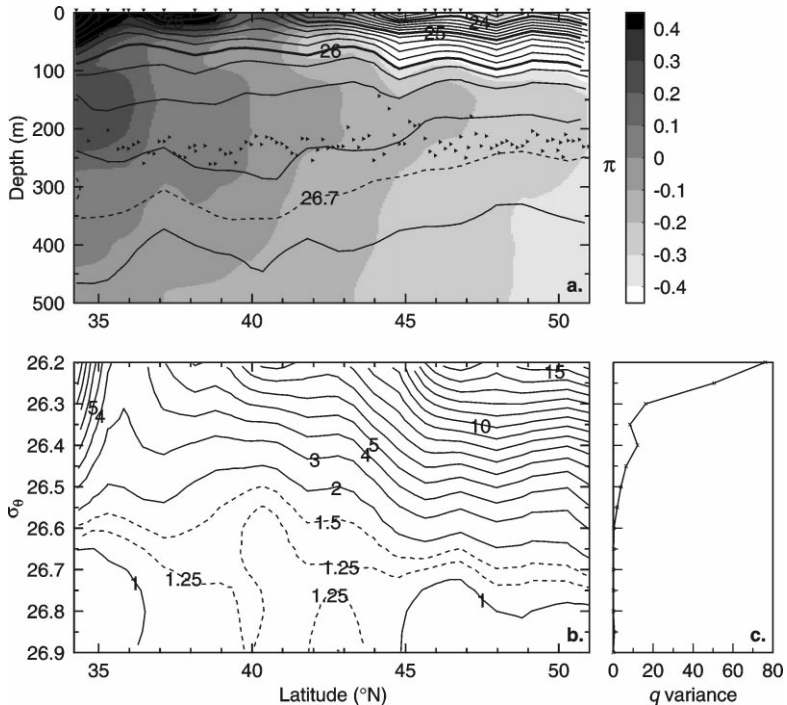
Fig. 8. (a) Vertical along-slope section using NMFS CTDs (station locations indicated at top). Contours are σ_θ, gray shade is spiciness π. The small triangles indicate the depth of the center of mass of poleward flow for each NMFS ADCP section. (b) Potential vorticity q (10^{-12} cm^{-1} s^{-1}) at σ_θ levels. (c) Variance of potential vorticity over the whole latitude range, for each σ_θ level.

250 m, consistent with historical estimates of undercurrent depth (Neshyba et al., 1989). In Pierce et al. (1996), we noted a slight poleward deepening of z_{cm}, but in that case we included poleward flow shallower than the 125 m level. In particular, the southern California bight region has significant poleward flow shallower than 125 m, sometimes called the Southern California countercurrent, which led to the conclusion of poleward deepening. Excluding this flow, which is probably a different dynamical phenomenon, z_{cm} has no apparent trend with latitude (Fig. 8a). Given the expected poleward shallowing of isopycnals, we note a general trend of the undercurrent core from $\sigma_\theta \sim 26.6$ water at 35°N to $\sigma_\theta \sim 26.7$ at 50°N. This is consistent with an undercurrent that mixes with slightly denser water downslope and offshore.

Isopycnic potential vorticity defined as $q = \rho^{-1} f \partial \rho / \partial z$, where f is the Coriolis parameter, calculated from hydrographic data in the manner of Talley (1988), can be a useful tracer of oceanic circulation. We calculate q using $\Delta\rho$ increments of 0.05 (Fig. 8b and 9b). Shallower than the $\sigma_\theta = 26.3$ level, we note strong meridional variability in q (Fig. 8c). At the $\sigma_\theta = 26.6$ level and deeper, the variance of q drops dramatically close to zero, and we note a broad region of reduced q variability centered about
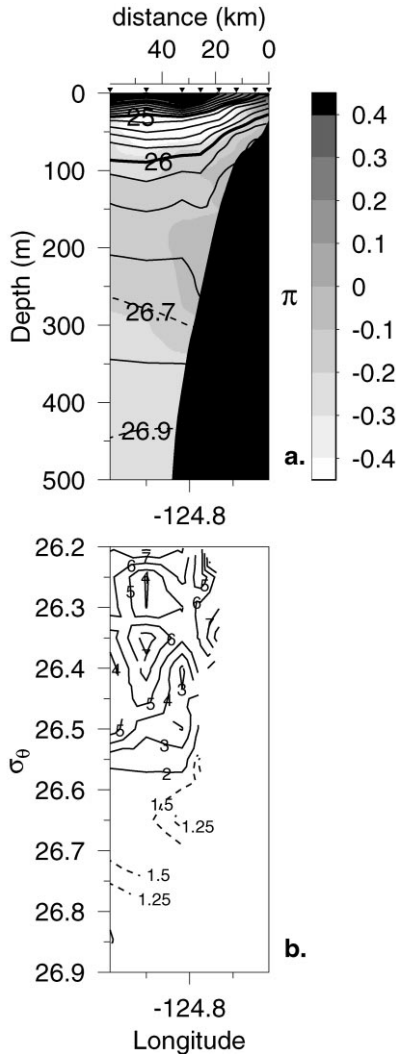
Fig. 9. (a) Cross-slope section at 43.2°N (the FM line) during the Cape Blanco study, CTD station locations indicated at top. Contours are σ_θ, gray shade is spiciness π. (b) Potential vorticity q (10^{-12} cm^{-1} s^{-1}) at σ_θ levels.

$q = 1.25 \times 10^{-12}$ cm^{-1} s^{-1}. This level of q is at $\sigma_\theta = 26.6$ at the southern end and $\sigma_\theta = 26.7$ at the northern end, consistent with z_{cm} as well as the spreading core of spiciness (Fig. 8a). Thus q appears to be a good tracer for the poleward undercurrent flow. In our cross-slope section as well (Fig. 9b), we see that the poleward undercurrent flow overlaps with the broad region of $q = 1-1.5 \times 10^{-12}$ cm^{-1} s^{-1} between 26.6 and 26.7.

This should not be surprising, since if we believe some part of the undercurrent to be continuous over this great range of latitude, it must have some mechanism for conserving its potential vorticity in the face of the significant change in planetary vorticity f. The way the undercurrent conserves q is by a slight thickening, a poleward increase in Δz between isopycnals, to counteract increasing f. Although we have neglected the effects of relative vorticity, we expect this to be a possibly important term in the undercurrent only in a local sense.

6. Summary

From this extensive set of NMFS ADCP data collected during July–August 1995, with supporting evidence from the intensive Cape Blanco study in August 1995, an improved view of the poleward undercurrent emerges. The undercurrent is present along almost the entire mid-latitude eastern boundary of the North Pacific, with a mean maximum velocity of $0.18\,\mathrm{m\,s}^{-1}$, overall mean of $0.10\,\mathrm{m\,s}^{-1}$, core depth 200–275 m, mean location 20–25 km off the shelf break, width of about a Rossby radius, and 125–325 m transport of $0.8 \pm 0.2 \times 10^6\,\mathrm{m}^3\,\mathrm{s}^{-1}$. ADCP streamfunction maps derived from velocity observations between Cape Blanco, Oregon, and Cape Mendocino, California, show some continuity of the undercurrent over this 440 km long region. In other portions of the flow, undercurrent water appears to leave the slope, thus breaking continuity on scales greater than about 300 km, in the form of anticyclonic eddies or as a portion of a separated equatorward jet in the vicinity of Cape Blanco. Analysis of alongshore hydrographic data provides additional evidence of continuity, particularly at levels below $\sigma_\theta = 26.6$–26.7. Potential vorticity in the range 1–$1.5 \times 10^{-12}\,\mathrm{cm}^{-1}\,\mathrm{s}^{-1}$ appears to be a good tracer of the poleward flow.

Acknowledgements

References

Akima, H., 1996. Rectangular-grid-data surface fitting that has the accuracy of a bicubic polynomial. ACM Transactions on Mathematical Software 22, 357–361.

Allen, J.T., Smeed, D.A., 1996. Potential vorticity and vertical velocity at the Iceland-Faeroes front. Journal of Physical Oceanography 26, 2611–2634.

Barnes, S.L., 1994. Applications of the Barnes objective analysis scheme, part III: tuning for minimum error. Journal of Atmospheric and Oceanic Technology 11, 1459–1470.

Barth, J.A., Pierce, S.D., Smith, R.L., 2000. A separating coastal upwelling jet at Cape Blanco, Oregon and its connection to the California Current System. Deep-Sea Research II 47, 783–810.

Barth, J.A., Smith, R.L., 1998. Separation of a coastal upwelling jet at Cape Blanco, Oregon, USA. South African Journal of Marine Science 19, 5–14.

Carter, E.F., Robinson, A.R., 1987. Analysis models for the estimation of oceanic fields. Journal of Atmospheric and Oceanic Technology 4, 49–74.

Chelton, D.B., deSzoeke, R.A., Schlax, M.G., El Naggar, K., Siwertz, N., 1998. Geographical variability of the first-baroclinic Rossby radius of deformation. Journal of Physical Oceanography 28, 433–460.

Collins, C.A., Garfield, N., Paquette, R.G., Carter, E., 1996a. Lagrangian measurement of subsurface poleward flow between 38°N and 43°N along the west coast of the United States during summer, 1993. Geophysical Research Letters 23, 2461–2464.

Collins, C.A., Paquette, R.G., Ramp, S.R., 1996b. Annual variability of ocean currents at 350-m depth over the continental slope off Pt. Sur, California. CalCOFI Reports 37, 257–263.

Cummins, P.F., Vallis, G.K., 1994. Algorithm 732: solvers for self-adjoint elliptic problem in irregular two-dimensional domains. ACM Transactions Mathematical Software 20, 247–261.

Daley, R., 1991. Atmospheric Data Analysis. Cambridge Press, Cambridge, 457pp.

Firing, E., Ranada, J., Caldwell, P., 1995. Processing ADCP data with the CODAS software system version 3.1, User's manual. (Manual and software available electronically at ftp://noio.soest.hawaii.edu/pub/codas3.)

Flament, P., 1986. Finestructure and subduction associated with upwelling filaments. Ph.D. Thesis, University of California, San Diego.

Garfield, N., Collins, C.A., Paquette, R.G., Carter, A., 1999. Lagrangian exploration of the California undercurrent, 1992–1995. Journal of Physical Oceanography 29, 560–583.

Hawkins, H.F., Rosenthal, S.L., 1965. On the computation of streamfunctions from the wind field. Monthly Weather Review 93, 245–252.

Howell, J.F., 1995. Identifying sudden changes in data. Monthly Weather Review 123, 1207–1212.

Huyer, A., 1980. The offshore structure and subsurface expression of sea level variations off Peru, 1976–77. Journal of Physical Oceanography 10, 1755–1768.

Huyer, A., Barth, J.A., Kosro, P.M., Shearman, R.K., Smith, R.L., 1998. Upper-ocean water mass characteristics of the California Current, summer 1993. Deep-Sea Research 45, 1411–1442.

Kosro, P.M., 1985. Shipboard acoustic profiling during the Coastal Ocean Dynamics Experiment. Ph.D. Thesis, SIO Ref. 85-8, Scripps Institute of Oceanography, La Jolla, CA, 119pp.

Kosro, P.M., Ramp, S.R., Smith, R.L., 1994. Moored current measurements over the continental slope in EBC: a first look. Transactions, American Geophysical Union, EOS 75 (44), 345.

Neshyba, S.J., Mooers, C.N.K., Smith, R.L., Barber, R.T. (Eds.), 1989. Poleward Flows along Eastern Ocean Boundaries. Springer, New York.

Pierce, S.D., Smith, R.L., Kosro, P.M., 1996. Observations of the poleward undercurrent along the eastern boundary of the mid-latitude Pacific. Transactions, American Geophysical Union, EOS 77 (46), F345.

Pierce, S.D., Barth, J.A., Smith, R.L., 1997. Acoustic Doppler Current Profiler observations during the Coastal Jet Separation project on R/V Wecoma, 17–27 August 1995. College of Oceanic and Atmospheric Sciences, Oregon State University, Data Rep. 166, Ref. 97-4, 123pp.

Pierce, S.D., 1997. Observations of the poleward undercurrent along the eastern boundary of the mid-latitude Pacific. [Data report, available on-line from http://diana.oce.orst.edu.]

Pollard, R., Read, J., 1989. A method for calibrating ship mounted acoustic Doppler profilers and the limitations of gyro compasses. Journal of Atmospheric and Oceanic Technology 6, 859–865.

Pollard, R., Regier, L., 1992. Vorticity and vertical circulation at an ocean front. Journal of Physical Oceanography 22, 609–625.

Smith, R.L., 1995. The physical processes of coastal upwelling systems. In: Summerhayes, C.P., Emeis, K.-C., Angel, M.V., Smith, R.L., Zeitzshel, B. (Eds.), Upwelling in the Ocean: Modern Processes and Ancient Records. Wiley, New York, pp. 39–64.

Talley, L.D., 1988. Potential vorticity distribution in the North Pacific. Journal of Physical Oceanography 18, 89–106.

Tibby, R.B., 1941. The water masses off the west coast of North America. Journal of Marine Research 4, 112–121.

Torgrimson, G.M., Hickey, B.M., 1979. Barotropic and baroclinic tides over the continental slope and shelf off Oregon. Journal of Physical Oceanography 9, 945–961.

Warren, B.A., 1990. Book review of Poleward flows along eastern ocean boundaries. Limnology and Oceanography 35, 1219–1220.

Wilson, C.D., Guttormsen, M.A., 1997. Echo integration-trawl survey of Pacific Whiting, Merluccius productus, off the west coasts of the United States and Canada during July–September 1995. NOAA Technical Memo NMFS-AFSC-74, NOAA-NMFS, US Department of Commerce.

Zedel, L.J., Church, J.A., 1987. Real-time screening techniques for Doppler current profiler data. Journal of Atmospheric and Oceanic Technology 4, 572–581.